

Synthesis and characterization of HAp/Fe₃O₄ Nanocomposites from Chicken Bone as a potential bone implant

*Aura Gitta Zhafirah*¹, *Dika Putra Wijaya*¹, *Taufaul Lita Magfirda*¹, *Marshya Qurrotul Aini Wibowo*¹, *Nilna Inayatan Nafiah*¹, *Putri Azzahra*¹, *Etika Sholichatus Zahroh*¹, *Yoshie Stephanie*¹, *Danar Danar*^{1,1}

¹Universitas Negeri Malang, Chemistry Department, 65145, Malang, Indonesia

Abstract. This study aims to synthesize and characterize hydroxyapatite/magnetite (HAp/Fe₃O₄) nanocomposites derived from chicken bones as potential materials for bone implants and eco-friendly adsorbents. Synthesis was conducted using the sol-gel method with calcination temperatures varied of 500°C, 600°C, and 700°C. Characterization was performed using XRD, FTIR, SEM-EDX, UV-Vis, and AAS. XRD results showed that at 700°C, a pure hydroxyapatite phase was formed with the highest crystallinity reaching 96.25% and a crystallite size of 20.14 nm, indicating an increase in the regularity of the crystal structure. FTIR analysis confirmed the presence of typical HAp functional groups (O–H and PO₄³⁻) as well as Fe–O groups from Fe₃O₄, indicating the successful formation of stable HAp/Fe₃O₄ magnetic composites at high temperatures. SEM-EDX results showed a porous morphology with particle sizes ranging from 4–20 nm, while AAS analysis shows a decrease in Ca ion content with increasing temperature, indicating an increase in the efficiency of HAp crystal structure formation. Furthermore, UV-Vis data showed an increase in absorbance at 200 nm with a value of 3.11 and a concentration of 0.816 ppm, indicating higher purity and structural regularity. Overall, the HAp/Fe₃O₄ nanocomposite at 700°C has high thermal stability, good crystal structure, and great potential for application as an environmentally friendly biomaterial.

1 Introduction

Bone injuries, particularly those resulting from accidents, remain a leading cause of hard tissue abnormalities worldwide. In 2019, global statistics estimated that 178 million bone fractures occurred. Indonesia specifically reports 1.3 million bone fracture cases annually, the highest incidence in Southeast Asia, with 119 hip fracture cases per 100,000 people each year. While surgical intervention, the standard treatment, carries risks including infection and nerve damage. Consequently, the development of safer, more effective technologies for bone

¹ Corresponding author: danar.fmipa@um.ac.id

biomaterial implantation has become a critical priority for restoring optimal bone function [1].

Biomaterials serve as substrates that facilitate tissue development while maintaining structural integrity and compatibility with biological systems. These synthetic materials, utilized in implants and medical devices, interact directly with biological environments to support, replace, repair, or restore physiological function. Essential properties include osteoconductivity, bioactivity, biocompatibility, and the absence of adverse inflammatory responses [2]. Additionally, biomaterials must be non-toxic, possess adequate fatigue strength, and exhibit high corrosion resistance. Hydroxyapatite (HAp) bioceramics are considered superior to other types due to their efficacy in promoting bone regeneration. The development of HAp-based biomaterials offers significant potential for enhancing bone and tissue restoration by enabling seamless integration with biological tissues [3].

Hydroxyapatite (HAp) is a biomimetic substitute material with chemical and structural properties closely resembling those of human bone. Its bioactivity facilitates bone fusion without adverse effects, while its biocompatibility ensures seamless integration with bodily tissues. HAp and β -tricalcium phosphate (β -TCP) are the primary calcium phosphate-based synthetic bone replacement materials, extensively studied and widely utilized for treating bone defects [4]. As a bioactive ceramic, HAp is fundamental constituent of hard tissues such as teeth and bones and demonstrating considerable potential for tissue regeneration and repair. Consequently, its relevance in tissue engineering and modern medicine continues to expand. The term hydroxyapatite generally refers to a family of crystalline minerals with the general formula $M_{10}(ZO_4)_6X_2$, where various ions can substitute for M, ZO_4 , and X components [5].

2 Method

2.1 Tool and Material

The tools needed in this research include standard laboratory glassware, oven, stainless steel autoclave tube, hot plate stirrer, magnetic stirrer, XRD (PANalytical X'Pert PRO), XRF (PANalytical Minipal 4), SEM-EDX (FEI Inspect-S50), AAS (ICE™ 3500), FTIR (Shimadzu IRPrestige 21), UV-Vis (Agilent Cary 60) instruments. The materials needed for the research included cleaned chicken bones, 0.06 M $Na_2HPO_4 \cdot 2H_2O$ solution (Merck), 25 % ammonia solution (Merck), 0.1 M Na_2EDTA solution (Merck), iron(II) chloride tetrahydrate ($FeCl_2 \cdot 4H_2O$) (Merck), iron(III) chloride hexahydrate ($FeCl_3 \cdot 6H_2O$) (Merck), 3 % H_2O_2 solution (Merck), isatin (LAB), resorcinol (Sigma Aldrich), sodium cyanoacetate (Merck), 37 % p.a. fuming HCl solution (Merck), distilled water, KBr powder (Merck), 96 % ethanol (Smartlab), and filter paper.

2.2 Synthesis of Hydroxyapatite from Chicken Bones

Chicken bone were collected from Among Farmers Central Market in Malang. Chicken bone underwent an initial cleaning process in boiling water at 100°C for 5 hours to remove the fat in the chicken bone that were still attached. The chicken bone that had been boiled for 6 hours were cleaned using distilled water and soaked in a 3% H_2O_2 solution for 5 hours. Then rinsed with distilled water and dried for 7 hours in an oven at 100°C. The dried chicken bones were weighed and subjected to calcination in a furnace with various temperatures of 500°C, 600°C, and 700°C for 5 hours. The resulting calcination results were then ground into powder using a mortar and pestle. The calcination product obtained in powder form was dissolved with distilled water and then characterized using an AAS instrument. The product yield from

the calcination process was determined by comparing the change in sample mass to the initial mass using Equation 1 with the following formula:

$$\% \text{ CaO} = \frac{\text{Mass after calcination}}{\text{Mass before calcination}} \times 100\% \quad (1)$$

The synthesis of hydroxyapatite required 50 mL of 0.1 M EDTA solution and 0.06 M $\text{Na}_2\text{HPO}_4 \cdot 2\text{H}_2\text{O}$ solution. In this synthesis, 2.8 grams of CaO were dissolved in 50 mL of 0.06 M $\text{Na}_2\text{HPO}_4 \cdot 2\text{H}_2\text{O}$ solution. Then, 50 mL of 0.1 M Na_2EDTA solution was added to the mixture at a rate of 4 mL/minute. The mixture was stirred using a hotplate stirrer for 1 hour at 400 rpm and heated to 100°C. The resulting precipitate was washed with distilled water until the pH was neutral and dried in an oven at 40°C for 24 hours to obtain a white powder. The resulting powder was characterized using FTIR and XRD [6].

2.3 Synthesis of Magnetite Fe_3O_4

Magnetite (Fe_3O_4) were produced using a conventional co-precipitation technique from $\text{Fe}^{2+}/\text{Fe}^{3+}$ salts. $\text{FeCl}_2 \cdot 4\text{H}_2\text{O}$ and $\text{FeCl}_3 \cdot 6\text{H}_2\text{O}$ were dissolved in deionized water at a molar ratio of $\text{Fe}^{2+} : \text{Fe}^{3+} = 1:2$ (total Fe approximately 0.4 M). The solution was heated to 70–80°C under a nitrogen atmosphere and subjected to vigorous stirring. Concentrated NH_4OH was cautiously introduced dropwise into the iron solution until a pH of approximately 10 was achieved. Black precipitates of Fe_3O_4 formed instantaneously upon basification. The mixture was maintained at an elevated temperature for 30 minutes to facilitate particle growth. The precipitate was subsequently decanted using a magnet and subjected to repeated washing with hot water and ethanol until a neutral pH was achieved, effectively removing chloride ions. The obtained magnetite was dried at 60°C overnight [7].

2.4 Synthesis of HAp/ Fe_3O_4 Nanocomposites

The synthesis of HAp/ Fe_3O_4 nanocomposites with a 1:1 composition was carried out by dissolving 0.5 grams of Fe_3O_4 in ethanol with the addition of 0.5 grams of hydroxyapatite powder. The sample mixture was then stirred for 1 hour using a hotplate stirrer at 400 rpm and heated to 130°C. After the mixing process was completed, the composite powder was formed. The next step was stirring with a magnetic stirrer for 24 hours. The composite powder was separated from the solution and washed with distilled water until the pH was neutral. The composite powder was dried in an oven at 80°C for 12 hours to obtain the HAp/ Fe_3O_4 nanocomposite. The resulting powder was characterized using FTIR and XRD.

2.5 Characterization of HAp/ Fe_3O_4 Nanocomposites

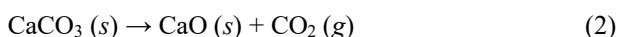
Characterization of hydroxyapatite quantitative include measurement of XRD (crystallinity index, crystallite size, highest peak d-spacing, and 2-theta HAp), XRF (chemical compound content in chicken bone), SEM (morphology and pore size distribution), FTIR (functional group), AAS (Ca metal content), and UV-Vis (band gap and phosphate absorbance results).

3 Result and Discussion

Hydroxyapatite (HAp) has the chemical formula $\text{Ca}_{10}(\text{PO}_4)_6(\text{OH})_2$. Its synthesis process requires the main precursors, calcium and phosphate, to form a thermodynamically stable crystal structure [8]. Calcium oxide (CaO) plays an important role as a calcium source in the synthesis of HAp. In this study, CaO was obtained by calcining chicken bone waste, a natural

source of calcium. The calcination process converts the sample's crystal phase to a more stable, highly crystalline phase, such as CaO [8]. Using chicken bone waste not only reduces waste but also produces calcium oxide in a more environmentally friendly way. This aligns with efforts in materials science to identify alternative raw materials that are more sustainable, while minimizing environmental impacts through recycling unused organic materials.

The content of chicken bones is 99.5% calcium carbonate, 0.23% Sc metal, and 0.47% Sr metal [8]. In this study, cleaned chicken bones were ground and calcined at 500°C, 600°C, and 700°C for 5 hours to decompose organic compounds and convert calcium carbonate (CaCO₃) into calcium oxide (CaO) by releasing carbon dioxide (CO₂). The calcination result showed that the CaO powder was white with different yields at each temperature. At 500°C, the yield was 97.32%; at 600°C, it was 74.53%; and at 700°C, it decreased to 74.39%. This process shows that the higher the calcination temperature, the lower the yield, likely due to the greater volatility of organic components and deeper decomposition at higher temperatures. The reaction equation for the chicken bone calcination process is shown in Equation 2.



Chicken bones were pulverized and calcined at 500°C, 600°C, and 700°C to break down organic components and calcium carbonate (CaCO₃) into calcium oxide (CaO) by releasing carbon dioxide (CO₂). The CaO produced by calcination is used in the synthesis of hydroxyapatite. CaO is mixed with the EDTA solution, which functions as a chelating reagent or complexing reagent. The EDTA solution binds Ca²⁺ to form a Ca-EDTA complex. The next step is the addition of Na₂HPO₄·2H₂O solution, which aims to release Ca²⁺ ions from the Ca-EDTA complex. The free Ca²⁺ ions can then interact with OH⁻ ions produced by water ionization, forming a hydroxyapatite structure. In addition, Ca²⁺ ions also bind to phosphate ions (PO₄³⁻) derived from Na₂HPO₄, forming hydroxyapatite crystal nuclei. These crystal nuclei then grow further in an oven during heating, which removes water and produces hydroxyapatite powder in the form of dry deposits.

Chicken bone samples were characterized using XRF to determine the elemental and compound composition of the chicken bones before and after calcination. This aimed to determine the percentages of elements and oxides in chicken bones, ensuring that Ca was dominant or higher than the others. The characterization results are listed in Table 1. The CaO content detected in the chicken bones after calcination ranged from 61.1% to 65.8%. The highest CaO content in the chicken bones was observed at 700°C (65.8%), indicating significant potential to increase the adsorbent capacity of HAp/ Fe₃O₄. Before calcination, the CaO content was found to be 92.84% [8].

Table 1. Comparison of chicken bone composition before and after calcination at 500-700°C.

No	Oxide	Before Calcination	After Calcination (500 °C)	After Calcination (600 °C)	After Calcination (700 °C)
1.	CaO	92.84 %	61.1 %	64.3 %	65.8 %
2.	Other oxide	7.16 %	38.9 %	35.7 %	34.2 %

Data Table 1 XRF analysis shows significant changes in the oxide composition of chicken bones after calcination at various temperatures (500°C, 600°C, and 700°C). Before calcination, the main content detected was CaO at 92.84%, which is the dominant element in the form of calcium phosphate (apatite), which is the main component of bone tissue. The high CaO content indicates that chicken bone minerals are composed of hydroxyapatite [Ca₁₀(PO₄)₆(OH)₂], which is a stable form of calcium phosphate [9]. After calcination, the percentage of CaO decreased to 61.1% at 500°C, then slightly increased to 64.3% and 65.8% at 600°C and 700°C, respectively. This decrease can be explained by the initial decomposition

of organic compounds and the evaporation of carbonates, leading to a significant increase in the relative abundance of other elements, such as P_2O_5 . The increase in phosphorus (P_2O_5) content from 0.98% to 27.6-29.8% after calcination indicates that phosphate becomes more dominant as the organic phase is removed, favoring the formation of a purer crystalline hydroxyapatite phase [10].

In addition to CaO and P_2O_5 , minor elements such as K_2O , SO_3 , and ZnO also experience a relative increase after calcination. The K_2O content increases from 0.41% to approximately 7.4% at 500°C, likely due to residual minerals or inorganic salts remaining after the organic matter degrades. ZnO and Fe_2O_3 remained present at low levels (< 1%), indicating that these metal oxides were not significantly affected by the heat treatment up to 700°C. The presence of these minor oxides can act as dopants, affecting the functional properties of calcined bone materials, for example, in bioceramic or catalyst applications. The most striking change was the loss of the most volatile elements, such as Cl and Sr, after calcination, indicating that these elements evaporated or decomposed at high temperatures. The stable Al_2O_3 (around 3.73%) indicates that aluminum did not react significantly during heating. In general, increasing the calcination temperature led to a simpler mineral composition, dominated by CaO and P_2O_5 indicating greater hydroxyapatite phase purity. Thus, the XRF results show that the calcination process plays an important role in degrading organic compounds and enriching inorganic mineral phases, especially CaO and P_2O_5 . Optimum conditions appear to be reached at 600-700°C, where the Ca/P ratio approaches the stoichiometric value of hydroxyapatite (Ca/P = 1.67). This indicates that chicken bones calcined at this temperature can serve as a potential raw material for the manufacture of bioceramics or as an environmentally friendly adsorbent.

3.1 Hydroxyapatite Synthesis

In this study, UV-Vis analysis was used to determine parameters such as phosphate that affect the stability and purity of the material. In addition, the concentration value (ppm) was measured to see the effect of calcination temperature on the amount of dissolved compounds or residues remaining in the sample. The following table shows the results of UV-Vis testing on HAp samples at three variations of calcination temperatures, namely 500°C, 600°C, and 700°C. UV-Vis test to determine the wavelength of phosphate (PO_4). The samples used in this test use the filtrate results from the HAp temperature variation of 500°C, 600°C, and 700°C [11]. The standard curve for calcium metal was $Y = 0.2655x - 0.0092$ with an R^2 of 0.9999. Depicts the differences in phosphate concentration levels using a UV-Vis spectrophotometer as follows Table 2.

Table 2. Depicts the differences in phosphate concentration levels using a UV-Vis spectrophotometer

Sample	Parameter	Wavelength (λ)	Absorbance	Concentration (ppm)
HAp 500 °C	Phosphate	400 nm	1.86 A	0.484
HAp 600 °C	Phosphate	400 nm	2.10 A	0.548
HAp 700 °C	Phosphate	400 nm	2.23 A	0.582

Characterization by UV-Vis at 400 nm showed that increasing the calcination temperature significantly affected the phosphate absorbance in hydroxyapatite (HAp) samples. The HAp sample heated to 500°C had an absorbance of 1.86 A, then increased to 2.10 A at 600°C, and reached a maximum of 2.23 A at 700°C. In UV-Vis measurements, absorbance is strongly influenced by the amount of phosphate-reagent complex formed; thus, an increase in absorbance indicates an increase in phosphate in the test solution. The correlation between absorbance and phosphate concentration is evident in the concentration values calculated from the calibration curve: 0.484 ppm (500°C), 0.548 ppm (600°C), and 0.582 ppm (700°C), respectively. The 13-20% increase in phosphate concentration aligns

with the Beer-Lambert law, which states that concentration is directly proportional to absorbance at a given wavelength. This indicates that changes in calcination temperature affect the amount of phosphate dissolved or detected after sample extraction.

Structurally, HAp calcined at higher temperatures exhibits increased crystallinity and phase stability. Increasing the calcination temperature can rearrange Ca^{2+} and PO_4^{3-} ions within the HAp crystal lattice, resulting in a more ordered structure. A more crystalline structure can lead to more pronounced phosphate release when the sample reacts with a phosphate-dye reagent, thereby increasing the UV-Vis signal. This is consistent with reports that calcination at 600-700°C increases HAp crystallinity and alters its surface properties. Furthermore, the temperature effect can also remove bound water and organic or carbonate components that may remain in the synthetic HAp structure [11]. The removal of these impurity groups increases HAp purity and makes phosphate groups more dominant in the structure, thereby making them easier to detect using colorimetric methods. Thus, increasing the calcination temperature can directly improve phosphate purity. AAS test to determine the concentration of calcium metal (Ca) in a filtrate from HAp filtration. The sample used in this test is HAp filtration filtrate at 500°C, 600°C, and 700°C. The standard curve for calcium metal was $Y = 0.01572x + 0.0011$ with an R^2 of 0.9998. The difference in calcium concentration using the AAS Table 3.

Table 3. Data calcium concentration in a filtrate hydroxyapatite

Test	Absorbance	Calcium Concentration (ppm)
HAp 500 °C	0.77 A	13.20 ± 0,01
HAp 600 °C	0.27 A	5.34 ± 0,01
HAp 700 °C	0.20 A	4.24 ± 0,01

The results of the AAS test showed a decrease in absorbance and calcium ion (Ca) concentration with increasing calcination temperature. At a temperature of 500°C, the measured absorbance value was 0.77 A with a calcium concentration of 13.20 ± 0.01 ppm, indicating that most of the Ca ions were still in the free phase (filtrate) because they had not fully bound to the phosphate group (PO_4^{3-}) to form a stable hydroxyapatite structure. This could be caused by the low crystallization rate and the presence of residual $\text{Ca}(\text{OH})_2$ precursors that had not been completely converted to $\text{Ca}_{10}(\text{PO}_4)_6(\text{OH})_2$. When the calcination temperature was increased to 600°C, the absorbance decreased sharply to 0.27 A, and the calcium concentration decreased to 5.34 ± 0.01 ppm. This decrease indicates that most of the Ca ions had bound to the phosphate to form a more regular HAp crystal network. The calcination process at medium temperatures encourages increased ion diffusion and the formation of a more homogeneous crystal phase, thus decreasing the dissolved Ca concentration in the filtrate. In other words, the lower the Ca content in the solution, the higher the efficiency of solid HAp structure formation.

At 700°C, the absorbance value drops again to 0.20 A, with a calcium concentration of 4.24 ± 0.01 ppm. This value indicates that almost all Ca ions are firmly bound in the HAp crystal structure. High temperatures accelerate crystal growth, increase densification, and strengthen the ionic bonds between Ca^{2+} and PO_4^{3-} . The decrease in Ca content in the filtrate strengthens the indication that high-temperature calcination increases the purity and stability of the hydroxyapatite phase. These results are consistent with previous research that found that increasing the calcination temperature improves HAp crystallinity and reduces free metal ions in the liquid phase [11]. In general, the decreasing trend in Ca concentration indicates the effectiveness of the calcination process in converting the precursor into a more perfect hydroxyapatite phase. This also shows that the calcination temperature directly influences the chemical interactions between Ca and phosphate ions, thereby determining the structure, stability, and functional properties of HAp. At too low a temperature, the structure is unstable; however, at an optimal temperature (around 700°C), HAp is formed with the high

purity and crystallinity desired for bioceramic and biomaterial applications. Thus, this AAS data confirms the results of previous UV-Vis tests that showed an increase in the order and stability of the HAp structure with increasing temperature. The correlation between the decrease in free Ca and the increase in optical absorbance indicates that the calcination process effectively improves the quality of the HAp material by increasing its purity and crystallinity.

XRD (X-ray Diffraction) is an effective analytical method for identifying the crystal structure of materials, including hydroxyapatite (HAp) extracted from chicken bone. Based on research by Kamilia [7], the XRD spectra were similar, with high intensities indicating high HAp crystallinity. HAp has a characteristic diffraction pattern according to COD ID number 9011091 (Hydroxyapatite) at 31.76, 32.19, 32.89, 34.06, 35.45, 38.16, with the main index (hkl): (-230), (-131), (-231), (-122). Increasing the temperature causes the peak intensity to increase and the peak width to decrease, which theoretically can increase the crystallinity of HAp. The Figure 1 shows the X-ray diffraction (XRD) patterns of HAp samples calcined at 500°C, 600°C, and 700°C, compared to the standard hydroxyapatite pattern (COD ID 9011091). In general, the diffraction patterns indicate that the primary phase is hydroxyapatite (HAp), but with differences in peak intensity and sharpness due to the calcination temperature and the presence of substitutions or interactions with HAp.

In the HAp sample at 500°C, the diffraction pattern shows relatively broad and less sharp peaks. This indicates that the resulting material still has a low degree of crystallinity and contains some amorphous phases. However, the typical HAp peak begins to appear at an angle of $2\theta = 31.7^\circ$, which is characteristic of the (211) diffraction plane in the HAp structure. This indicates that the HAp phase has formed, but the crystal structure has not fully developed due to insufficient thermal energy to form a stable crystal lattice. As the calcination temperature increases to 600°C, the diffraction peaks become more intense and sharper, especially in the range $2\theta = 31.7^\circ$ - 32.9° . This indicates an increase in crystallinity, meaning the HAp crystal structure is becoming more regular. At this temperature, the recrystallization process becomes more effective, resulting in a more dominant HAp phase and higher phase purity than at 500°C.

The diffraction pattern of HAp at 700°C shows the sharpest and most intense peaks among the three temperatures. This indicates that HAp has the highest crystallinity at this temperature, meaning its crystal structure has fully developed. The main peak at $2\theta \approx 31.7^\circ$ becomes more prominent, indicating that the pure HAp phase becomes very dominant, in accordance with the standard pattern of COD ID 9011091. This increase in calcination temperature also increases crystallite size, consistent with the general result that higher heating temperatures lead to larger particle sizes due to crystal growth. Based on the related XRD results table, increasing the calcination temperature directly affects crystallinity (%) and crystallite size (nm). The crystallinity value increases from about 79.96% at 500°C to 84.17% at 700°C (the table data strengthens the same trend for 500-700°C). Meanwhile, the crystallite size also increased from 15.21 nm to approximately 23.9 nm, indicating grain growth due to the high thermal energy. Although the data table lists temperatures above 700°C, the trend of increasing crystallinity and crystallite size remained consistent throughout the 500-700°C range.

Overall, these results confirm that increasing the calcination temperature from 500°C to 700°C results in a significant change in the HAp crystal structure, from amorphous to crystalline. The major peaks, which match the standard HAp pattern, demonstrate that the primary phase formed remains hydroxyapatite, with no strong indication of impurities such as β -tricalcium phosphate (β -TCP) or CaO. From an application perspective, these results demonstrate that HAp calcined at 700°C has the highest purity and crystallinity, making it an ideal candidate for biomedical applications such as bone implants or tissue engineering materials. However, if the application requires higher bioactivity, HAp with moderate

crystallinity, such as at 600°C, may be more suitable due to its more reactive surface. Thus, these XRD results not only demonstrate the development of the crystal structure but also provide a basis for selecting the optimal calcination temperature based on the HAp application requirements Table 4 and Figure 1 [3].

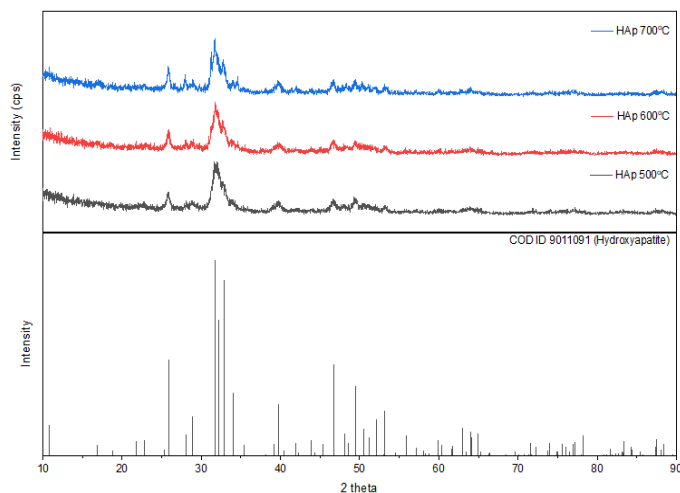


Figure 1. Peak XRD result of HAp 500 °C, 600 °C, and 700 °C

Table 4. XRD analysis results for HAp 500 °C, 600 °C, and 700 °C

No	Sample	2 θ deg	d(\AA)	Crystallinity (%)	Crystalline Size (nm)
1.	HAp 500°C	29.42°	3.03539	79.960	15.2091
2.	HAp 600°C	31.71°	2.82129	80.945	16.6324
3.	HAp 700°C	31.89°	2.80591	84.171	23.9049

The infrared transmittance spectrum of the HAp composite was generated and shown in Figure 2. This spectrum shows the presence of PO_4^{3-} groups detected at several frequency ranges, namely 1022.27-1045.41 cm^{-1} , 879.54 cm^{-1} . Meanwhile, carbonate (CO_3^{2-}), which plays an important role in tissue engineering due to its bioactivity and reabsorption properties similar to the composition of human bone, was detected at around 1411.89-1415.75 cm^{-1} . The decrease in the intensity of the CO_3^{2-} peak began at 1000°C due to carbonate decomposition. In addition, in the calcination process at temperatures of 500°C, 600°C, and 700°C, there was a decrease in the intensity of the OH^- group at around 3500-3600 cm^{-1} , which was caused by the dehydroxylation process of the OH^- group Table 5 and Figure 2.

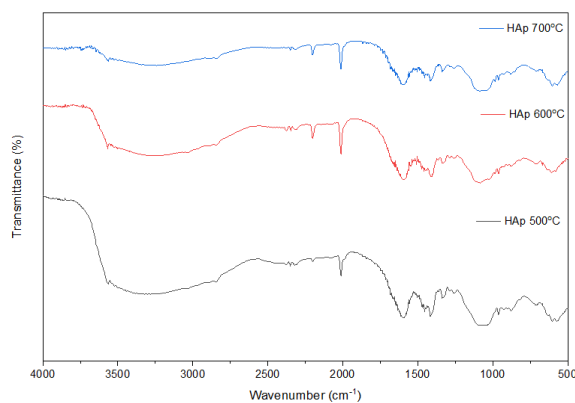


Figure 2. FTIR peak result of HAp 500°C, 600°C, and 700°C (19)**Table 5.** FTIR wave number results of HAp 500°C, 600°C, and 700°C (19)

Vibration	Wavenumber (cm ⁻¹)				
	HAp 500°C	HAp 600°C	HAp 700°C	Reference HAp	Ref.
O-H	3564.45	3568.30	3562.52	3634 and 3448	[6]
C-H	2845	2845	2837.28	-	-
-C=O	2011.75	2011.75	2011.75	-	-
C=O	1415.75	1411.89	1415.75	1418	[6]
-PO ₄	1045.41 and 879.54	1022.27 and 879.54	1045.41 and 879.54	1045 and 874	[6]

The FTIR analysis results shown in Figure 2 and Table 5 indicate that the main absorption band at 3560 cm⁻¹ corresponds to the stretching vibrations of the hydroxyl (-OH) groups, characteristic of the HAp crystal structure. These peaks appear, respectively, at 3564.45 cm⁻¹ (HAp 500 °C), 3568.30 cm⁻¹ (HAp 600 °C), and 3562.52 cm⁻¹ (HAp 700 °C). The presence of these bands indicates that the hydroxyl groups remain stable up to 700°C, although a slight shift in peak position suggests a change in the crystal environment or partial dehydroxylation at higher temperatures. This phenomenon is consistent with reports that higher temperatures can reduce the number of OH groups by releasing air from the HAp lattice. Furthermore, a weak absorption band around 2845–2837 cm⁻¹ indicates the presence of C-H vibrations from residual organic compounds or alkyl groups, possibly derived from precursor synthesis. The decrease in the intensity of the C–H band at 700°C indicates the decomposition of organic residues during calcination, thereby increasing the purity of HAp.

The absorption bands at 2011.75 cm⁻¹ (C=O) and 1415.75 cm⁻¹ (C–O) indicate the possible presence of carbonate (CO₃²⁻) groups substituted in the HAp crystal lattice. This common carbonate substitution occurs during synthesis using organic solvents or materials, or during heating when CO₂ is absorbed from the atmosphere. Carbonate groups replacing phosphate or hydroxyl groups produce characteristic bands in the 1410–1470 cm⁻¹ and 870–890 cm⁻¹ regions, which are also observed in the 700°C HAp sample. This indicates that carbonate remains trapped within the HA structure despite increasing heating temperatures and may play a role in determining the material's bioactivity and solubility. A characteristic phosphate (PO₄³⁻) band was detected around 1045 cm⁻¹ and 1022 cm⁻¹, which corresponds to the asymmetric stretching vibration (ν_3) of the phosphate group. These values align with the typical reference peaks of pure HAp in the 1045–1090 cm⁻¹ range (Markovic et al., 2004). The presence of an additional band around 879 cm⁻¹ in HAp at 700°C indicates a change in the phosphate ion environment due to increased crystallinity and a reduction in lattice defects. The tendency for the PO₄³⁻ band to shift to higher wavenumbers with increasing temperature indicates that the HAp structure becomes more ordered and crystalline. Overall, the FTIR results confirm that all samples contain the typical HAp groups, namely -OH and PO₄³⁻, with an additional carbonate band indicating minor substitution. Heating to 700°C increases the regularity of the crystal structure by removing organic components, but also causes slight dehydroxylation. The shift and sharpening of the vibration bands indicate an increase in HAp crystallinity with increasing calcination temperature, consistent with previous studies on the thermal effects on the stability and structure of synthetic hydroxyapatite [12].

SEM testing was conducted to determine the surface structure and pore diameter of the HAp sample. The SEM test results showed the surface morphology of the porous hydroxyapatite sample at calcination temperatures of 500°C, 600°C, and 700°C. In the SEM test, the hydroxyapatite sample showed temperature-dependent changes at 500°C (Figure 3), 600°C (Figure 7), and 700°C (Figure 11).

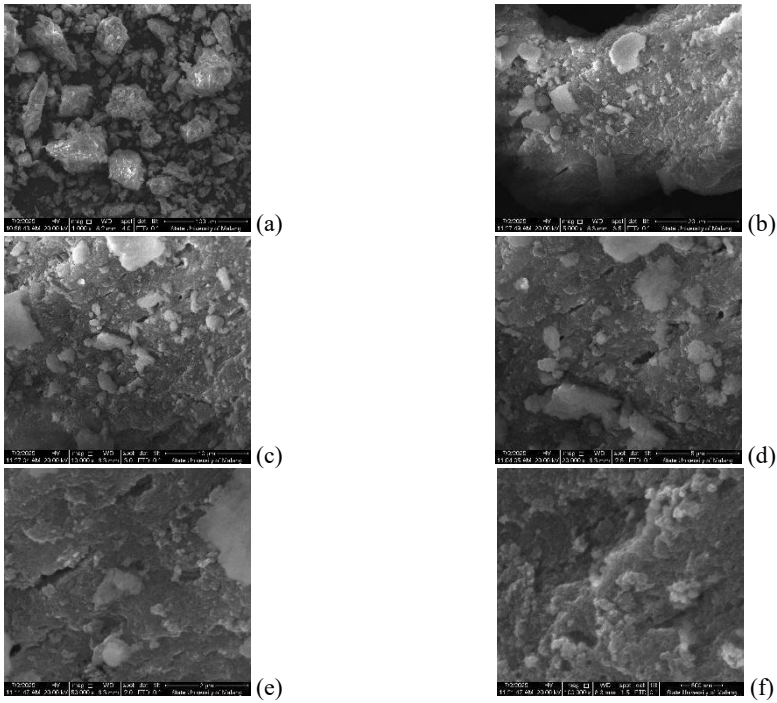


Figure 3. Morphology of hydrothermally synthesized HAp 500 °C with magnifications a) 1.000x, b) 10.000x, c) 10.000x, d) 20,000, e) 50,000x, f) 100,000x

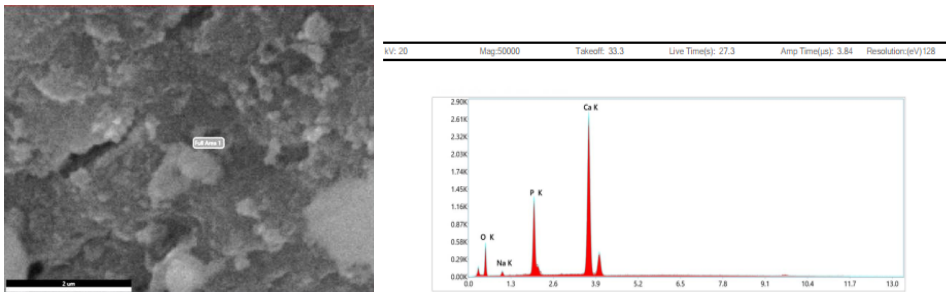


Figure 4. SEM-EDX HAp 500 °C result in Area 1

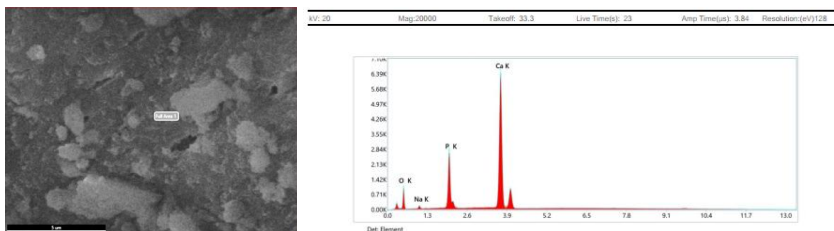


Figure 5. SEM-EDX HAp 500 °C result in Area 2

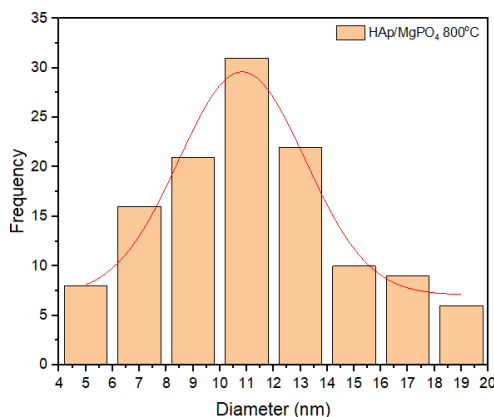


Figure 6. HAp 500 °C nanocomposite particle size distribution with 100.000x magnification image

Figure 3 shows that the calcination temperature can affect the pore diameter size of the hydroxyapatite sample, which tends to have porous properties. The pore diameter size of the porous hydroxyapatite sample can be measured using the scale line in the SEM test result image. After measuring the pore diameter of the hydroxyapatite sample, the average pore diameter was 4-20 nm. The characterization result using SEM at a magnification of 1,000-100,000x visually shows that the morphology formed is a porous material. If observed more closely, it can be seen that the size formed is in the nanometer range. SEM photo observations also reveal the irregular, even porosity. Furthermore, SEM-EDX analysis reveals the elemental composition of the pure HAp sample from chicken bone. The SEM-EDX result shows a temperature variation of 500°C, Figure 4 (Area 1) and Figure 5 (Area 2)

In particle analysis using SEM, Image refraction was performed to determine the particle diameter of the HAp nanocomposite. The SEM analysis results from ImageJ refraction are shown in Figure 6. Based on particle testing using SEM and ImageJ refraction, the size of the hydroxyapatite composite in chicken bone and magnesium phosphate ranges from 4 to 20 nm, which can be categorized as a nanocomposite. Nanocomposites are materials with a composite size below 100 nm or less than 1 μm [13]. This is supported by a reference that defines nanocomposites as composites with a size of 4-20 nm, illustrated with a 100,000x magnification image. The results of the EDX spectrum of HAp in area 1 (Figure 4) show the presence of inorganic elements in the HAp formation, consisting of Ca 30.45%, P 4.47%, Si 1.26%, Na 13.68%, and several organic elements, such as O 50.13%. The results of the EDX spectrum of HAp in area 3 (Figure 5) show the presence of inorganic elements in the HAp formation, consisting of Ca 100%. These results indicate that in HAp with a temperature variation of 600°C, there is HAp formation content (Ca, P, Si, Na, and O).

Figure 7 show that the calcination temperature can affect the pore diameter size of the hydroxyapatite sample which tends to have porous properties. The pore diameter size of the porous hydroxyapatite sample can be measured using the scale line in the SEM test result image. After measuring the pore diameter on the hydroxyapatite sample, the pore diameter size was obtained with an average of 10-60 nm. The characterization result using SEM at a magnification of 1.000-100.000x visually shows that the morphology formed is a porous material. If observed more closely, it can be seen that the size formed is in the nanometer range. The result of SEM photo observations also show the porosity formed which is irregular and even. Furthermore, the result of SEM-EDX observations show the elements contained in the pure HAp/Fe₃O₄ sample from chicken bone. The SEM-EDX result a temperature variation of 900°C Figure 8 (Area 1) and Figure 9 (Area 2)

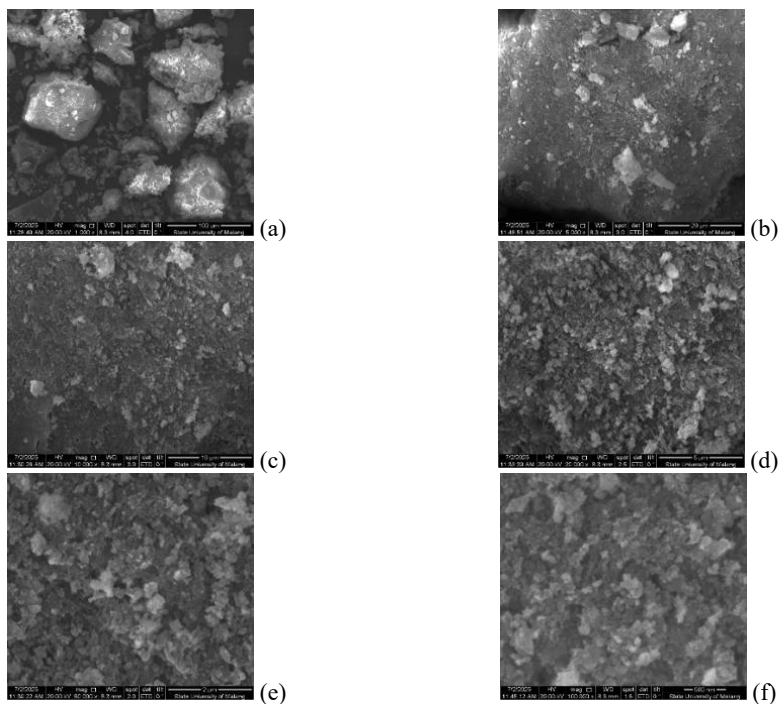


Figure 7. Morphology of hydrothermally synthesized HAp 600°C with magnifications a) 1.000x, b) 10.000x, c) 20,000, d) 50,000x, e) 100.000x

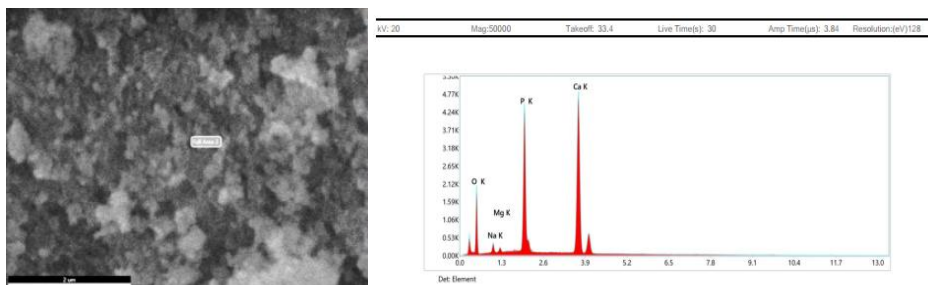


Figure 8. SEM-EDX HAp 600°C result in Area 1

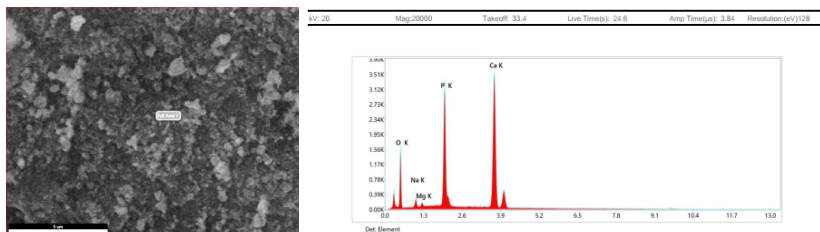


Figure 9. SEM-EDX HAp 600°C result in Area 2

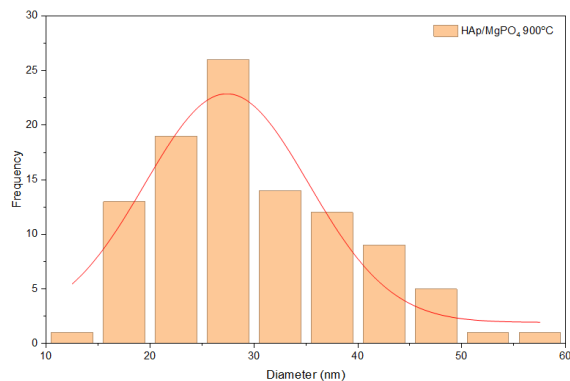


Figure 10. HAp 600°C nanocomposite particle size distribution with 100.000x magnification image

In particle analysis using SEM, ImageJ refractive index was used to determine the particle diameter of the HAp/Fe₃O₄ nanocomposite. The SEM analysis results from ImageJ refraction are shown in Figure 10. Based on particle testing using SEM and ImageJ refraction, the size of the hydroxyapatite composite in chicken bone and magnesium phosphate ranges from 10 to 60 nm, which can be categorized as a nanocomposite. Nanocomposites are materials with a composite size below 100 nm or less than 1 μm [13]. This is supported by a reference that defines nanocomposites as composites with a size between 10-60 nm, illustrated with a 100,000x magnification image. The results of the EDX spectrum of HAp in area 1 (Figure 8) show the presence of inorganic elements in the HAp formation, consisting of Ca 33.72%, P 0.89%, Mg 0.24%, and several organic elements, such as O 65.15%. The results of the EDX spectrum of HAp in area 2 (Figure 9) show the presence of inorganic elements in the HAp formation, consisting of Ca 36.51%, P 0.83%; P 0.83%, and organic elements such as O 62.49%, and several elements with low intensity, such as Na 0.2% and Mg 0.2%. These results indicate that in HAp with a temperature variation of 900°C, there is HAp formation content (Ca, P, Mg), as well as organic content (O).

Figure 11 shows that the calcination temperature can affect the pore diameter size of the hydroxyapatite sample, which tends to have porous properties. The pore diameter size of the porous hydroxyapatite sample can be measured using the scale line in the SEM test result image. After measuring the pore diameter on the hydroxyapatite sample, the average pore diameter was 15-100 nm. The characterization result using SEM at a magnification of 1,000-100,000x visually shows that the morphology formed is a porous material. If observed more closely, it can be seen that the size formed is in the nanometer range. SEM photo observations also reveal the irregular, even porosity. Furthermore, SEM-EDX analysis shows the elements present in the pure HAp/Fe₃O₄ sample from chicken bone. The SEM-EDX result shows a temperature variation of 1000°C, Figure 12 (Area 1) and Figure 13 (Area 2).

In particle analysis using SEM, ImageJ refractive index correction was applied to determine the particle diameter of the HAp nanocomposite. The SEM analysis results from ImageJ refraction are shown in Figure 14. Based on particle testing using SEM and ImageJ refraction, the size of the hydroxyapatite composite in chicken bone and magnesium phosphate ranges from 15 to 100 nm, which can be categorized as a nanocomposite. Nanocomposites are materials with a composite size below 100 nm or less than 1 μm [13]. This is supported by reference, which defines nanocomposites as composites with a size of 5-25 nm, as shown in a 100,000x magnification image. The results of the EDX spectrum of HAp in area 1 (Figure 8) show the presence of inorganic elements in the HAp formation, consisting of Ca 55.01%, P 3.52%, and several organic elements, such as O 41.47%. The results of the EDX spectrum of HAp in area 2 (Figure 9) show the presence of inorganic elements in the HAp formation, consisting of Ca 38.22%, P 3.19%, organic elements such as

O 58.59%, and several elements with low intensity, such as Na 0.2% and Mg 0.2%. These results indicate that in HAp with a temperature variation of 1000°C, there is HAp formation content (Ca, P), as well as organic content (O).

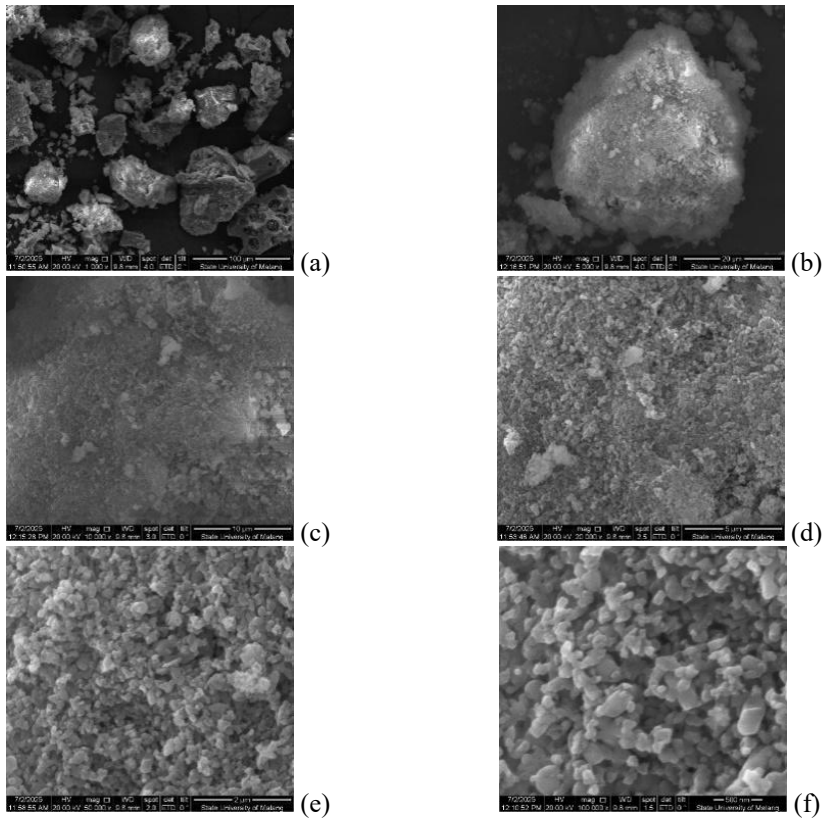


Figure 11. Morphology of hydrothermally synthesized HAp 700°C with magnifications a) 1.000x, b) 10.000x, c) 20,000, d) 50,000x, e) 100.000x

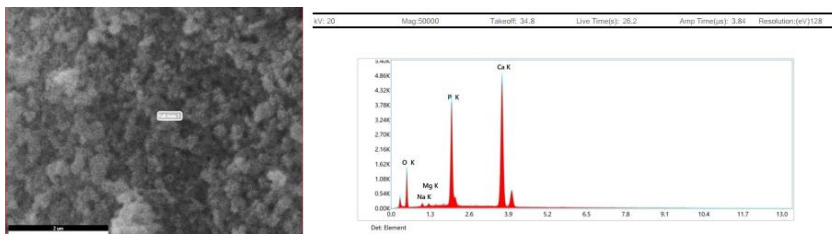


Figure 12. SEM-EDX HAp 700°C result in Area 1

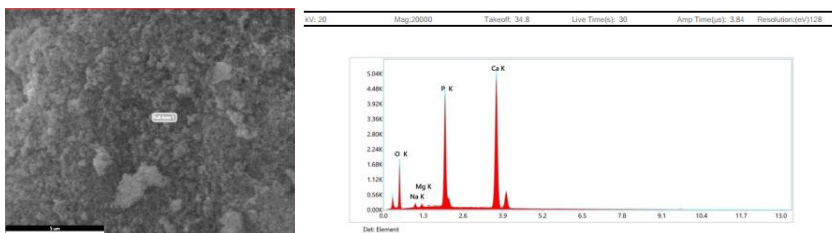


Figure 13. SEM-EDX HAp 700°C result in Area 2

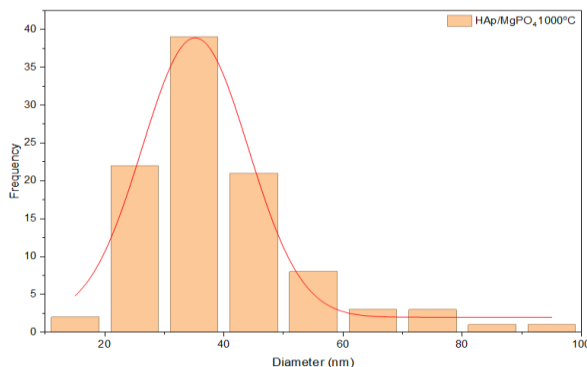
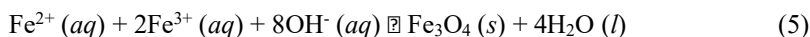


Figure 14. HAp 700°C nanocomposite particle size distribution with 100.000x magnification image

3.2 Fe₃O₄ synthesis

Synthesis of magnetite (Fe₃O₄) from a ratio of Fe²⁺ and Fe³⁺ of 2:1. The addition of ammonia to the mixture between the solutions of Fe²⁺ and Fe³⁺ ions can cause the formation of magnetite deposits to recur, so a stoichiometric reaction equation is required, as shown in Equation 5.



UV-Vis DRS test to determine the concentration of band gap, charge transfer, d-d transition of transition metals, and the purity of the magnetite sample. The samples used were magnetite samples. The results of the standard curve on the UV-Vis spectrophotometer were $Y = 0.2655x + 0.0092$ with R^2 of 0.9999. The absorbance and concentration of each parameter in the hydroxyapatite samples of 500°C, 600°C, and 700°C, as shown in Table 6, are:

Table 6. UV-Vis DRS concentration data on magnetite samples

Sample	Parameter	Wavelength (λ) in nm	Absorbance (A)	Concentration Parameter (ppm)
Fe ₃ O ₄	Band Gap	200 nm	2,65	0,730 ± 0,01
	Transfer Change	250 nm	1,57	0,432 ± 0,01
	d-d Transition	400 nm	1,15	0,316 ± 0,01
	Purity	800 nm	1,13	0,312 ± 0,01

The results of the UV-Vis DRS spectrophotometer test on the magnetite (Fe₃O₄) sample provide an in-depth overview of its optical properties and electronic structure. Based on the test results, the highest absorbance peak occurs at 200 nm, with a concentration of 0.730 ± 0.01 ppm. This peak indicates a band-to-band transition (band-gap transition), which describes the minimum energy required to promote an electron from the valence band to the conduction band. This phenomenon confirms that Fe₃O₄ exhibits semiconductor behavior with a small band gap, in line with previous reports that it has a band gap of around 2.0 eV [7]. At a wavelength of 250 nm, an absorbance peak of 0.432 ± 0.01 ppm was observed, identified as a charge transfer transition from O²⁻ to Fe³⁺ ions. This transition indicates a strong interaction between oxygen and iron ions in the magnetite crystal structure. This confirms the inverse spinel model of Fe₃O₄, where Fe²⁺ and Fe³⁺ ions alternately occupy octahedral and tetrahedral positions [9]. This charge interaction also plays a key role in determining the magnetic properties and electrical conductivity of Fe₃O₄, making it an attractive material for sensor and catalyst applications.

Furthermore, the peak at 400 nm with an absorbance of 0.316 ± 0.01 ppm corresponds to the d-d transition of Fe^{2+} and Fe^{3+} ions. This transition is characteristic of transition metal complexes and indicates the presence of iron ions in octahedral coordination. The relatively low absorbance in this region indicates that Fe_3O_4 has good optical purity. Another peak at 800 nm exhibits an absorbance of 0.312 ± 0.01 ppm, which is often used as a reference for assessing the optical purity of materials.

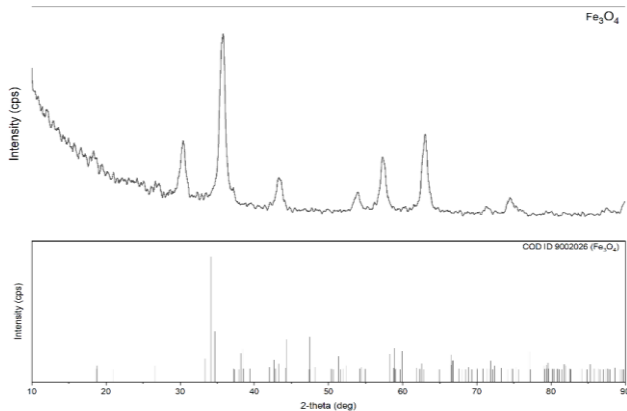


Figure 15. XRD peak results for Fe_3O_4

The X-ray diffraction (XRD) data displayed shows Table 7 and Figure 15 a typical magnetite (Fe_3O_4) diffraction pattern. Based on the measurement results, the main intensity peaks appear at 2θ angles of around 30° , 35.5° , 43° , 53° , 57° , and 62° , which correspond to the crystal planes (220), (311), (400), (422), (511), and (440). These peaks indicate the typical cubic spinel crystal structure of Fe_3O_4 , which has been widely reported in the literature as the dominant phase of magnetite [7]. When compared with the data standard (COD ID 9002026), the sample diffraction pattern results show excellent agreement. There were no significant changes in peak positions, indicating no changes in the crystal structure or the formation of other phases such as hematite ($\alpha\text{-Fe}_2\text{O}_3$) or maghemite ($\gamma\text{-Fe}_2\text{O}_3$). Therefore, it can be concluded that the synthesized sample has high phase purity and successfully formed a pure magnetite phase (Fe_3O_4). The relatively wide diffraction peak indicates that the Fe_3O_4 crystallite size is on the nanometer scale. According to the Scherrer equation, a smaller crystallite size leads to peak broadening due to increased diffraction effects in small particles. This is commonly found in Fe_3O_4 nanoparticles synthesized through coprecipitation or precipitation methods [7]. Furthermore, the highest intensity of the (311) peak indicates that this crystal plane is the dominant plane in the orientation of the Fe_3O_4 crystals. This is in line with the general characteristics of magnetite, which has a preferential orientation on the (311) plane. The strong relative intensity in this plane is also associated with good magnetic properties because the orientation affects the magnetic domains within the particle [14].

$$\text{Crystallinity} = \frac{\text{Crystalline area fraction}}{\text{Crystalline area fraction} + \text{amorphous area fraction}} \times 100\%$$

Table 7. XRD analysis results of Fe_3O_4 peak

No.	Sample	2θ deg	$d(\text{\AA})$	Crystallinity (%)	Crystal Size (nm)	Ref.
1.	m- Fe_3O_4	35.55°	2.53	-	28.93	[14]
2.	Fe_3O_4	35.77°	2.50987	82.243	9.5792	-

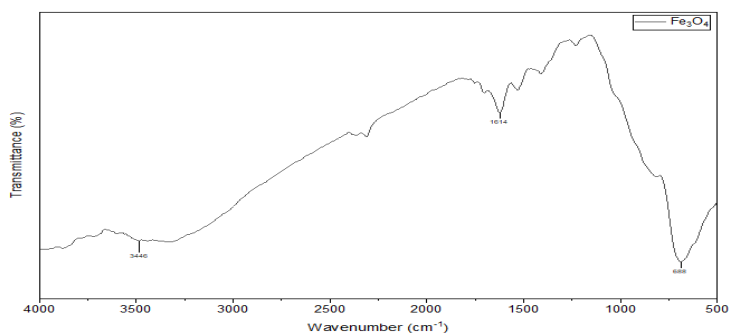


Figure 16. Fe₃O₄ FTIR Peak Results

The infrared transmittance spectrum of the Fe₃O₄ composite was generated and shown in Figure 16 and Table 8. This spectrum indicates the presence of an OH⁻ group at 3446.87 cm⁻¹. Subsequently, the CO₂ peak intensity of the double bond stretching vibration (C=O) was detected at 1614 cm⁻¹. This indicates that calcination temperature affects changes in magnetite's functional groups, as shown in Figure 16 and Table 8 [15].

Table 8. FTIR wave number results of Fe₃O₄

Vibration	Wavenumber (cm ⁻¹)		Reference
	Reference Fe ₃ O ₄	Synthesis Fe ₃ O ₄	
O-H	3400	3446,87	[14]
C=O	1636	1614,42	[14]
Fe-O	566	688,58	[14]

In this study, UV-Vis DRS analysis was used to determine parameters such as band gap, charge transfer, and the presence of inorganic groups such as phosphate, sulfate, fluoride, nitrate, and nitrite that affect the stability and purity of the material. In addition, the concentration value (ppm) was measured to see the effect of calcination temperature on the amount of dissolved compounds or residues remaining in the sample. The following table shows the results of UV-Vis testing on the HAp/ Fe₃O₄ sample at a calcination temperature of 700°C. UV-Vis test to determine the wavelength of phosphate (PO₄). The samples used in this test are the filtrate results from HAp at temperatures of 500°C, 600°C, and 700°C. The standard curve for calcium metal was $Y = 0.2655x - 0.0092$ with an R² of 0.9999. Depicts the differences in phosphate concentration levels using a UV-Vis spectrophotometer as follows Table 9.

Table 9. Depicts the differences in parameter concentration levels using a UV-Vis spectrophotometer

Sample	Parameter	Wavelength (λ)	Absorbance	Concentration (ppm)
HAp/Fe ₃ O ₄ 700°C	Phosphate	400 nm	2.47 A	0.646

The UV-Vis spectrophotometer test results table for the Fe₃O₄ sample shows various optical and chemical parameters measured over the wavelength range of 200-800 nm. The highest absorbance peak was observed at 200 nm, with an absorbance of 3.11 and a concentration of 0.816 ppm, corresponding to a band-gap transition. This peak indicates the transition of electrons from the valence band to the conduction band, a common phenomenon in semiconductor compounds such as Fe₃O₄. The band gap energy value reflects the material's ability to absorb photon energy for electron excitation, which also affects its optical properties and conductivity. At a wavelength of 250 nm with an absorbance of 2.69, this phenomenon is associated with a charge transfer transition between Fe²⁺ and Fe³⁺ ions in the magnetite spinel structure. This process indicates that Fe₃O₄ exhibits mixed semiconductor

behavior, in which electrons can move between metal centers with different oxidation states. This phenomenon is crucial because it relates to the unique magnetic and electronic properties of Fe_3O_4 , which make it superior for applications such as sensors, catalysts, and magnetic materials.

Another peak at 800 nm, with an absorbance of 2.40, indicates a d–d transition of the Fe^{2+} ion and thus an interaction between electrons in the d orbitals. This peak confirms that the Fe_3O_4 structure is composed of Fe ions in two different oxidation states, namely Fe^{2+} and Fe^{3+} , which contribute to its ferrimagnetic properties and the ability of electron conduction within the crystal lattice. The relatively high absorbance value in this region indicates the material's ability to absorb energy at high wavelengths (the NIR region) (Huang et al., 2016). The absorbance values for this parameter ranged from 2.26 to 2.93 at concentrations of 0.590–0.768 ppm, indicating that Fe_3O_4 is capable of interacting with various inorganic ions in solution. This demonstrates the adsorption potential of the Fe_3O_4 surface, which is often utilized for environmental applications such as the removal of heavy metals or harmful anions from water.

The color peak at 212 nm, with an absorbance of 2.93 at a concentration of 0.768 ppm, confirms the high optical transparency in the UV region, reflecting Fe_3O_4 's ability to efficiently absorb ultraviolet light. This phenomenon indicates strong optical activity arising from the interaction between photons and electrons at the nanoparticle surface, which contributes to the material's photocatalytic activity. Overall, these UV-Vis data demonstrate that Fe_3O_4 exhibits strong optical properties, including band-gap, charge-transfer, and d-d transitions. Furthermore, the presence of other inorganic components demonstrates the potential of this material for photocatalysis, ionic sensing, and environmental applications. Consistency in absorbance and concentration values demonstrates system stability and the material's ability to efficiently absorb electromagnetic radiation across a wide range of wavelengths.

AAS test to determine the concentration of calcium metal (Ca) in a filtrate from HAP filtration. The sample used in this test is HAp filtration filtrate at 500°C, 600°C, and 700°C. The standard curve for calcium metal was $Y = 0.01572x + 0.0011$ with an R^2 of 0.9998. The difference in calcium concentration using the AAS Table 9.

Table 9. Data calcium concentration in a filtrate hydroxyapatite

Test	Absorbance	Calcium Concentration (ppm)
HAp/ Fe_3O_4 700°C	0.77 A	13.20 ± 0.01

The results of the AAS test showed a decrease in absorbance and calcium ion (Ca) concentration with increasing calcination temperature. At a temperature of 500°C, the measured absorbance value was 0.77 A with a calcium concentration of 13.20 ± 0.01 ppm, indicating that most of the Ca ions were still in the free phase (filtrate) because they had not fully bound to the phosphate group (PO_4^{3-}) to form a stable hydroxyapatite structure. This could be due to the low crystallization rate and the presence of residual $\text{Ca}(\text{OH})_2$ precursors that have not been fully converted to $\text{Ca}_{10}(\text{PO}_4)_6(\text{OH})_2$. When the calcination temperature was increased to 600°C, the absorbance decreased sharply to 0.27 A, and the calcium concentration decreased to 5.34 ± 0.01 ppm. This decrease indicates that most of the Ca ions had bound to the phosphate to form a more regular HAp crystal network. The calcination process at medium temperatures encourages increased ion diffusion and the formation of a more homogeneous crystal phase, thus decreasing the dissolved Ca concentration in the filtrate. In other words, the lower the Ca content in the solution, the higher the efficiency of solid HAp structure formation.

At 700°C, the absorbance value drops again to 0.20 A, with a calcium concentration of 4.24 ± 0.01 ppm. This value indicates that almost all Ca ions are firmly bound in the HAp

crystal structure. High temperatures accelerate crystal growth, increase densification, and strengthen the ionic bonds between Ca^{2+} and PO_4^{3-} . The decrease in Ca content in the filtrate further supports the notion that high-temperature calcination increases the purity and stability of the hydroxyapatite phase. These results are consistent with previous research that found that increasing the calcination temperature improves HAp crystallinity and reduces free metal ions in the liquid phase. In general, the decreasing trend in Ca concentration indicates the effectiveness of the calcination process in converting the precursor into a more perfect hydroxyapatite phase. This also shows that the calcination temperature directly influences the chemical interactions between Ca and phosphate ions, thereby determining the structure, stability, and functional properties of HAp. At too low a temperature, the structure is unstable; however, at an optimal temperature (around 700°C), HAp is formed with the high purity and crystallinity desired for bioceramic and biomaterial applications. Thus, this AAS data confirms the results of previous UV-Vis tests that showed an increase in the order and stability of the HAp structure with increasing temperature. The correlation between the decrease in free Ca and the increase in optical absorbance indicates that the calcination process effectively improves the quality of the HAp material by increasing its purity and crystallinity.

The XRD results (Figure 17) show a major peak at $2\theta = 31.90^\circ$ with an interplane spacing (d) = 2.8051 Å, a value commonly associated with the major crystallographic peaks of hydroxyapatite (HAp) (usually a strong peak around $31\text{--}32^\circ$ for the (211)/(300) plane depending on the index convention). These favorable peak positions indicate a well-formed HAp phase in the sample after treatment up to 700°C ; the absence of a major shift in 2θ indicates that the HAp crystal lattice is relatively stable and that few substitutional ions alter its lattice parameters. The high crystallinity (96.252%) indicates that most of the material is in the crystalline HAp phase rather than the amorphous phase. An increase in crystallinity is common as the calcination temperature rises, as greater atomic mobility enables grain growth and the removal of disordered phases or organic residues. Therefore, the 96% crystallinity at 700°C indicates an efficient crystallization process for the analyzed sample.

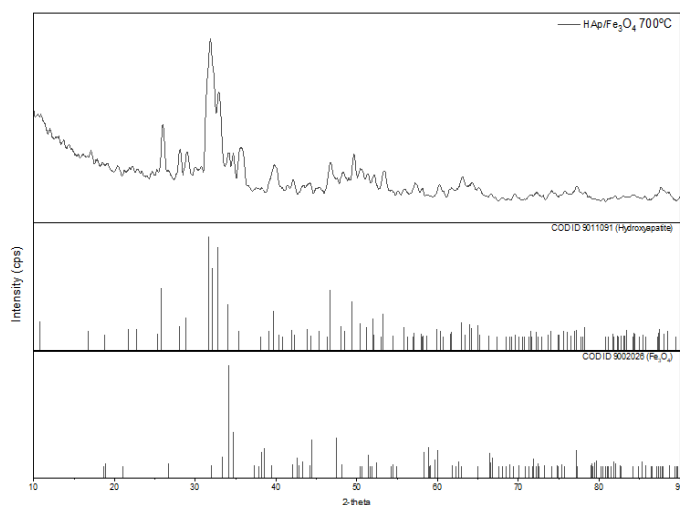


Figure 17. Peak XRD result of HAp/ Fe_3O_4 700°C

Table 10. XRD analysis results for HAp/ Fe_3O_4 700°C

No	Sample	2θ deg	$d(\text{\AA})$	Crystallinity (%)	Crystalline Size (nm)
1.	HAp/ Fe_3O_4 700°C	31.90	2.80510	96.252	20.144

The infrared transmittance spectrum of the HAp composite was generated and shown in Figure 18 and Table 11. This spectrum shows the presence of PO_4^{3-} groups detected at several frequency ranges, namely $1022.27\text{--}1045.41\text{ cm}^{-1}$, 879.54 cm^{-1} . Meanwhile, carbonate (CO_3^{2-}), which plays an important role in tissue engineering due to its bioactivity and reabsorption properties similar to the composition of human bone, was detected at around $1411.89\text{--}1415.75\text{ cm}^{-1}$. The decrease in the intensity of the CO_3^{2-} peak began at 1000°C due to carbonate decomposition. In addition, in the calcination process at temperatures of 500°C , 600°C , and 700°C , there was a decrease in the intensity of the OH^- group at around $3500\text{--}3600\text{ cm}^{-1}$, which was the dehydroxylation process of the OH^- [15].

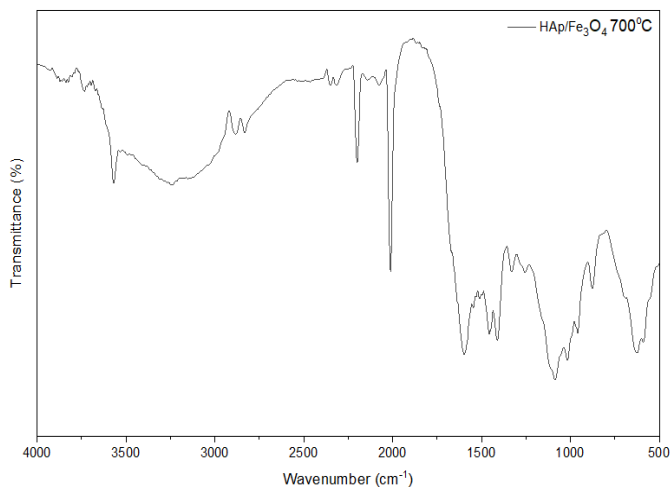


Figure 18. FTIR peak result of HAp/Fe₃O₄ 700°C

Table 11. FTIR wavenumber results of of HAp/Fe₃O₄ 700°C

Vibration	Wavenumber (cm ⁻¹)		
	Synthesis HAp/Fe ₃ O ₄ 700°C	Reference HAp/Fe ₃ O ₄	Reference
O-H	3568.30	3634 and 3448	[1]
C-H	2883.57	-	-
-C=O	2198.85	-	-
C=O	1408.03	1418	[1]
-PO ₄	1083.99 and 877.61	1045 and 874	[1]
Fe-O	588.28	566	[14]

FTIR spectrum of Table 11 and Figure 18 the HAp/Fe₃O₄ composite at 700°C displays several characteristic peaks indicating the presence of functional groups typical of hydroxyapatite (HAp) and magnetite (Fe₃O₄). The absorption peak at 3568.30 cm^{-1} indicates the presence of stretching vibrations of the O–H group, which is characteristic of the hydroxyl group in the HAp crystal structure. The presence of this band indicates that the hydroxyl group remains stable even after high-temperature calcination. This value is in line with references stating that the O–H band in HAp generally appears at a distance of $3634\text{--}3448\text{ cm}^{-1}$, indicating the consistency of the HAp structure in the composite. In addition, the appearance of a peak at 2883.57 cm^{-1} indicates the presence of a C–H group, which most likely originates from residual organic compounds or solvents during the synthesis process. Although not a primary characteristic of HAp, the presence of C–H groups is frequently found in biomineral-based materials resulting from wet chemical synthesis. This peak indicates that a small amount of organic matter remains in the structure, without disrupting the stability of the main groups in HAp or Fe₃O₄.

The absorption peaks at 2198.85 cm^{-1} and 1408.03 cm^{-1} indicate the presence of C=O and C–O groups, respectively, associated with the carbonate (CO_3^{2-}) anion. This indicates that some of the phosphate groups in HAp may have been substituted by carbonate ions, forming carbonate-hydroxyapatite (CHA). This substitution generally enhances the bioactivity and biological interaction capabilities of HAp, thus making this material composition potentially suitable for biomedical applications. According to [6], the appearance of carbonate groups after the calcination process also indicates that the reaction between HAp and Fe_3O_4 proceeds smoothly without compromising their fundamental properties. Furthermore, strong absorption bands at 1083.99 cm^{-1} and 877.61 cm^{-1} are the main characteristics of the phosphate group (PO_4^{3-}) in HAp. These peaks indicate the symmetric and asymmetric stretching vibrations of the phosphate group and confirm that the hydroxyapatite crystal structure remains stable at high temperatures. These values are close to the reference value in the range of $1045\text{--}874\text{ cm}^{-1}$, indicating the stability of the phosphate phase after calcination. The presence of these bands also indicates that the HAp phase does not decompose into calcium oxide or other undesirable compounds. Finally, the peak at 588.28 cm^{-1} indicates the presence of the Fe–O group, a characteristic of magnetite (Fe_3O_4). This peak corresponds to the reference value of 566 cm^{-1} reported by Nuryono [14]. The presence of this band indicates that magnetite has been successfully integrated into the HAp matrix without altering the primary chemical structures of either. The combination of the Fe–O and PO_4^{3-} peaks indicates that the HAp/ Fe_3O_4 composite is successfully formed homogeneously, resulting in a material with both magnetic and bioactive properties. Overall, these FTIR results show that the HAp/ Fe_3O_4 composite calcined at 700°C retains the main functional groups of each of its constituent components. The O–H and PO_4^{3-} groups prove the presence of HAp, while the Fe–O indicates the presence of magnetite.

SEM testing was conducted to determine the surface structure and pore diameter of the HAp sample. The SEM test results showed the surface morphology of the porous hydroxyapatite sample at calcination temperatures of 500°C , 600°C , and 700°C . In the SEM test, hydroxyapatite and magnetite samples showed evidence of phase transformation at 700°C (Figure 19).

Figure 19 shows that the calcination temperature can affect the pore diameter size of the hydroxyapatite sample, which tends to have porous properties. The pore diameter size of the porous hydroxyapatite sample can be measured using the scale line in the SEM test result image. After measuring the pore diameter of the hydroxyapatite sample, the average pore diameter was 4–20 nm. The characterization result using SEM at a magnification of 1,000–100,000x visually shows that the morphology formed is a porous material. If observed more closely, it can be seen that the size formed is in the nanometer range. SEM photo observations also reveal the irregular, even porosity. Furthermore, the results of SEM-EDX analysis show the elements present in the pure HAp sample from chicken bone. The SEM-EDX results show a temperature variation of 500°C in Figure 20 (Area 1), Figure 21 (Area 2), and Figure 22 (Area 3).

In particle analysis using SEM, ImageJ refractive index was used to determine the particle diameter of the HAp/ Fe_3O_4 700°C nanocomposite. The graph of the SEM analysis results performed with ImageJ refraction is shown in Figure 23. Based on particle testing using SEM and ImageJ refraction, the size of the hydroxyapatite composite in chicken bone and magnesium phosphate ranges from 4 to 20 nm, which can be categorized as a nanocomposite. Nanocomposites are materials with a composite size below 100 nm or less than $1\text{ }\mu\text{m}$ [13]. This is supported by reference, which defines nanocomposites as composites with a size of 4–20 nm, as shown in a 100,000x magnification image. The results of the EDX spectrum of HAp/ Fe_3O_4 700°C in area 1 (Figure 20) show the presence of inorganic elements in the formation consisting of Ca 14.35 %, P 10.91%, Mg 1.47%, Na 4.10%, Fe 1.33%, and several organic elements, such as O 67.84%. The results of the EDX spectrum of HAp/ Fe_3O_4 700°C

in area 2 (Figure 21) show the presence of inorganic elements in the formation consisting of Ca 15.42%; P 10.95%; Mg 0.79%; Na 3.84%; Fe 1.07%, and several organic elements, such as O 67.92%. The results of the EDX spectrum of HAp/Fe₃O₄ 700°C in area 3 (Figure 22) show the presence of inorganic elements in the formation consisting of Ca 26.27%, P 12.08%, Mg 0.37%, Na 4.10%, Fe 1.25%, K 0.10%, and several organic elements, such as O 67.84%. These results indicate that in HAp/Fe₃O₄ at 700°C, there is a formation content (Ca, P, Na, Mg, Fe, K, and O).

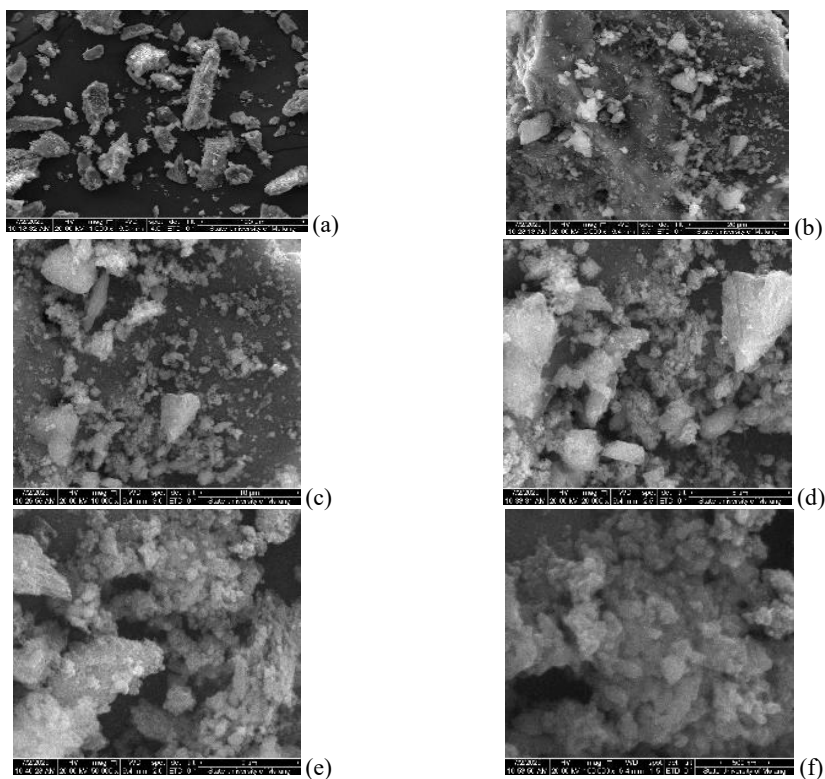


Figure 19. Morphology of hydrothermally synthesized HAp/Fe₃O₄ 700°C with magnifications a) 1.000x, b) 10.000x, c) 10.000x, d) 20,000, e) 50,000x, f) 100.000x

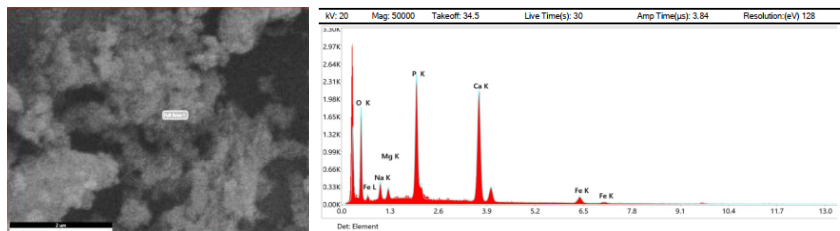


Figure 20. SEM-EDX HAp/Fe₃O₄ 700°C result in Area 1

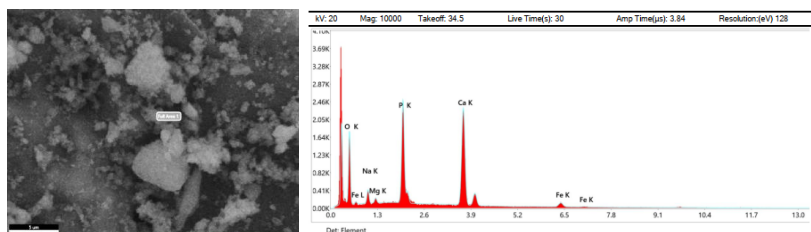


Figure 21. SEM-EDX HAp/Fe₃O₄ 700°C result in Area 2

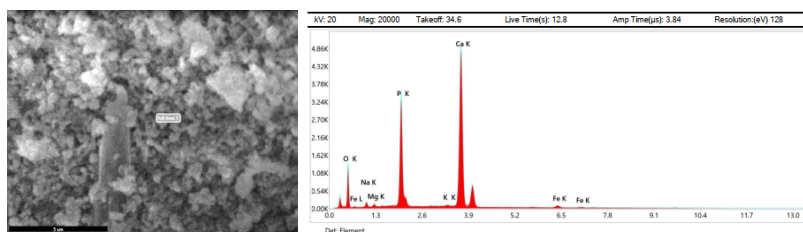


Figure 22. SEM-EDX HAp/Fe₃O₄ 700°C result in Area 3

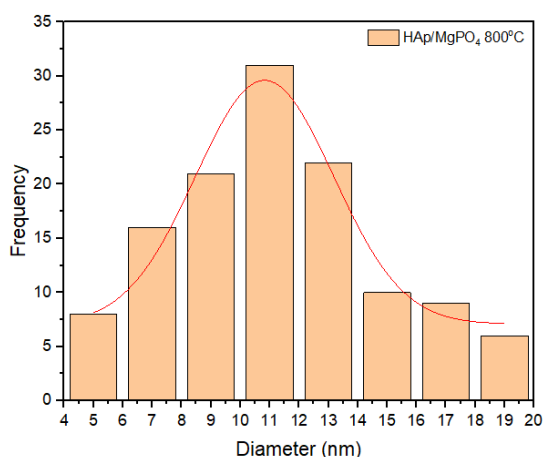


Figure 23. HAp/Fe₃O₄ 700°C nanocomposite particle size distribution with 100.000x magnification image

4 Conclusion

The results showed the findings demonstrate that HAp/Fe₃O₄ nanocomposites were successfully synthesized from chicken bone waste through calcination and high-temperature mixing with magnetite. XRD analysis identified 700°C as the optimal condition for forming hydroxyapatite with high crystallinity and nanometer-scale crystallites. FTIR spectra confirmed the presence of O-H and PO₄³⁻ groups characteristic of HAp, as well as Fe-O groups indicative of Fe₃O₄, signifying effective integration of both phases within the composite. SEM-EDX analysis revealed a porous morphology with nanometer-sized particles and a predominance of Ca, P, and Fe, consistent with the stoichiometric ratio of HAp/Fe₃O₄. UV-Vis analysis indicated increased absorbance with higher calcination temperatures, reflecting enhanced purity and structural regularity, while AAS results showed a reduction in free Ca content, suggesting improved efficiency in HAp/Fe₃O₄ formation.

Acknowledgement

We would like to acknowledge and thank the (1) Central Laboratory of State University of Malang, (2) The authors acknowledge and thank the internal funding at Universitas Negeri Malang for the research funding student innovation 24.2.912/UN32.14.1/LT/2025.

References

1. M. Davlet, K. Smyrnova, and A. Pogrebnyak, "Advanced biomaterials in tissue engineering: A critical review of nanocomposites based on bacterial cellulose, MXenes, hydroxyapatite, and metal particles for regenerative medicine," *Adv. Colloid Interface Sci.*, vol. **345**, p. 103634, Nov. 2025, doi: 10.1016/j.cis.2025.103634.
2. P. Zhang, Y. Nie, X. Wang, X. Zhang, and L. Liu, "Next-generation smart ophthalmic biomaterials: From passive response to active interaction and closed-loop control," *Bioact. Mater.*, vol. **56**, pp. 522–558, Feb. 2026, doi: 10.1016/j.bioactmat.2025.10.037.
3. M. Lauskis, O. Radzins, S. E. Uribe, S. Grybauskas, and G. Salms, "Volumetric stability of biphasic hap/ β -tcp/collagen implants in malar augmentation: A CBCT-Based case series after orthognathic surgery," *Journal of Cranio-Maxillofacial Surgery*, vol. **53**, no. 9, pp. 1530–1537, Sep. 2025, doi: 10.1016/j.jcms.2025.06.003.
4. B. Zhang *et al.*, "Extracellular matrix-mimetic enhanced porous bioscaffolds for accelerating bone defect repair," *Mater. Des.*, vol. **261**, p. 115301, Jan. 2026, doi: 10.1016/j.matdes.2025.115301.
5. Charlena, Nazriati, B. Marita Soebrata, and M. Dicky Iswara, "Synthesis and Characterization of Hydroxyapatite Composites Based on Tutut (Belamyia Javanica) and Magnetite by Coprecipitation as Adsorbents of Pb Metals Ion," *Science and Technology Indonesia*, vol. **10**, no. 1, pp. 111–122, Jan. 2025, doi: 10.26554/sti.2025.10.1.111-122.
6. A. R. Liandi, R. W. Sari, T. P. Wendari, Imelda, D. Febriantini, and A. Insani, "Hydroxyapatite/PCL/Fe₃O₄ waste-based composite: An efficient green catalyst for spirooxindole-chromene synthesis under ultrasonic irradiation," *Case Studies in Chemical and Environmental Engineering*, vol. **10**, p. 100892, Dec. 2024, doi: 10.1016/j.cscee.2024.100892.
7. S. Kamilia, F. Mukhayani, S. Sutarno, and N. Nuryono, "Modification of Chitosan-Coated Magnetic Material with Glycidyl-trimethylammonium Chloride for Cr(VI) Adsorption," *Indonesian Journal of Chemistry*, vol. **25**, no. 1, p. 244, Jan. 2025, doi: 10.22146/ijc.100749.
8. T. Haniastuti, V. M. Karina, P. K. Arindra, and R. K. Dewi, "Chicken Bone Hydroxyapatite Bone-Graft On Post-Exodontia Socket Healing (Angiogenesis)," *Int. Dent. J.*, vol. **74**, p. S159, Oct. 2024, doi: 10.1016/j.identj.2024.07.1061.
9. B. Bouzar, N.-E. Abriak, and M. Benzerzour, "Sustainable reuse of mineral waste: Synthesis and comprehensive characterization of hydroxyapatite (HAP)," *Green Technologies and Sustainability*, vol. **4**, no. 2, p. 100315, Apr. 2026, doi: 10.1016/j.grets.2025.100315.
10. R. Wu, Y. Wang, J. Wang, G. Tian, Y. Li, and C. Liu, "Facile preparation of Fe₃O₄/HAP/Ag nanomaterial and photocatalytic degradation of four types of dyes with mechanism," *RSC Adv.*, vol. **15**, no. 33, pp. 27128–27138, 2025, doi: 10.1039/D5RA03777H.
11. S.-C. Wu, H.-C. Hsu, L.-C. Ou, and W.-F. Ho, "Effects of hydrothermal temperature on the synthesis and characterization of bioactive hydroxyapatite nanoparticles from oyster shell," *Journal of the Australian Ceramic Society*, vol. **61**, no. 4, pp. 1525–1536, Sep. 2025, doi: 10.1007/s41779-025-01189-w.

12. R. Kareem and O. Kaygili, "Hydroxyapatite Biomaterials: A Comprehensive Review of their Properties, Structures, Medical Applications, and Fabrication Methods," vol. **6**, pp. 1–26, Jan. 2024, doi: 10.48309/JCR.2024.415051.1253.
13. J. Huang and L. Wang, "Recent advances in rare earth adsorption and recovery using Fe₃O₄-based functionalized core-shell magnetic nanomaterials: Challenges and perspectives," *J. Environ. Manage.*, vol. **397**, p. 128364, Jan. 2026, doi: 10.1016/j.jenvman.2025.128364.
14. J. N. Naat, S. Suyanta, and N. Nuryono, "Effectiveness comparison of octyltrimethoxysilane and hexadecyltrimethoxysilane functionalized on natural silica-coated magnetic materials for ciprofloxacin and chloramphenicol adsorption," *Mater. Adv.*, vol. **6**, no. 10, pp. 3220–3236, 2025, doi: 10.1039/D4MA01252F.
15. M. Pahlavansadegh, S. Bagdeli, and A. Taheri-Kafrani, "Hydroxyapatite-boosted Fe₃O₄ nanozymes with enhanced peroxidase-like activity for multiplex biosensing of ascorbic acid/uric acid and serum total antioxidant capacity," *Colloids Surf. A Physicochem. Eng. Asp.*, vol. **734**, p. 139346, Apr. 2026, doi: 10.1016/j.colsurfa.2025.139346.